Site-selectively grown SnO_2 NWs networks on micromembranes for efficient ammonia sensing in humid conditions

Jordi Samà[a], Sven Barth[b], Guillem Domènech-Gil[a], Joan-Daniel Prades[a], Núria López[c], Olga Casals[a] , Isabel Gràcia[d], Carles Cané[d], Albert Romano-Rodríguez[a*]

[a]*Universitat de Barcelona (UB), MIND-Departament of Electronics and Institute of Nanoscience and Nanotechnology (IN2UB), c/Martí i Franquès 1, E-08028 Barcelona, Spain*

[b]*Vienna University of Technology (TUW), Institut of Materials Chemistry, Getreidmarkt 9/BC/02, A-1060 Vienna, Austria*

[c]*Institute of Chemical Research of Catalonia (ICIQ), Av. Països Catalans 16, E-43007 Tarragona, Spain*

[d]*Consejo Superior de Investigaciones Científicas (CSIC), Institut de Microelectrònica de Barcelona (IMB-CNM), Campus UAB, E-08193 Bellaterra, Spain*

* Corresponding author. Tel.: +34-934039156.
E-mail address: aromano@el.ub.edu

Abstract

SnO_2 NWs networks on heated micromembranes have been characterized as ammonia sensors. The approach allows achieving reproducible growth and stable and long-lasting ammonia sensors with site-specific grown SnO_2 NWs. The devices have been tested both in dry and humid conditions showing response time down to two minutes. Sensors have been tested up to 1 month, only presenting variation of the base resistance with full retention of the response towards the gaseous analytes. Different concurrent sensing mechanisms have been identified relating the determined sensing kinetics with previous theoretical calculations. Specifically, oxygen dissociation seems to play a key role in the overall ammonia sensing sequence. In humid conditions, moisture reduces the response to ammonia but also lowers the activation energy of the reaction process.

1. Introduction

Ammonia is a toxic gas with irritant properties that can injure the respiratory tract [1]. Anthropogenic emissions mainly comes in a 95% from agriculture, where ammonium salts are widely used as a fertilizer [2]. On the other hand, swine farms can achieve high concentrations of ammonia up to 100 ppm generated by decomposition of pig manure via metabolic activities of bacteria and fungi [3].

Furthermore, ammonia, together with urea, is used in automotive applications for selective catalytic reduction (SCR) of nitrogen oxide (NO_x) to nitrogen in order to avoid harmful gas emissions in diesel heavy weight engines, which gives also H_2O as a byproduct [4,5]. Accurate measurements of the ammonia concentration for SCR are needed for an efficient process and the recycling of the non-reacted ammonia fraction.

SnO_2 and other metal oxides have been explored as chemo-resistive gas sensing materials since the development of Taguchi sensors four decades ago [6]. More recently, nanostructured metal oxide materials were developed in order to improve the sensing properties by enhancing the surface to volume ratio [7]. Among them, nanowires are one of the most studied and promising structures because of their well-controlled chemical and physical properties [8]. Nanowire-based gas sensors have been developed by using individual structures [9] or in a network form where the electrical current flows through the nanowires along the axial direction [10]. Single SnO_2 nanowire gas sensors have been demonstrated as sensitive and effective devices, but are constrained by *ad hoc* contact fabrication, which is time consuming and difficult to systematize.

A possibility for its industrial processing would be the alignment of nanowires using dielectrophoretic forces [11].

Monocrystalline SnO_2 structures offer better stability to gas response than multigrained ones because the former expose more stable, homogeneous and well defined crystal planes to gases. Single crystalline nanowires can be prepared by metal seed supported gas phase growth techniques, such as chemical vapor deposition (CVD) or pulsed laser deposition (PLD) [8]. The growth of nanowires often requires high temperatures; for instance, SnO_2 nanowires form around 700 °C [12]. The growth process according to the vapor-liquid-solid mechanism (VLS) is frequently performed by CVD, involving long times for heating up and cooling down due to the high thermal mass of the furnace; additionally, the entire heated substrate is coated and not only the active area. Consequently, the transfer of nanowires to the final device is required, adding complexity to the approach. Precise growth and integration of nanowires in an efficient and reproducible way is one of the most challenging aspects for gas sensors based on such structures.

Thus, nanostructures grown directly on the final electronic device severely reduces fabrication steps and manufacturing cost. At the same time, a low power consumption during the growth is achieved due to the small mass of the heated area allowing fast heating and cooling processes. The approach presented here is based on direct growth of nanowires onto micromembranes, small membrane areas of 400x400 µm with an incorporated heater that provides the temperature necessary for the growth of SnO_2 nanowires and for the sensor operation [13]. The nanostructures are available after the growth for resistor-type sensing applications without requiring any additional fabrication step due to the bridging of the interdigitate on top of the heater.

In this work, we present an ammonia sensor based on SnO_2 nanowires grown by this direct integration process of nanostructures with the electronic platform and their response in dry and humid air.

2. Experimental details

Bulk micromachined substrates were used as a platform for the growth of nanowires. Chips consist of 4 isolating micromembranes with a thickness about 1.1 µm with reduced thermal mass that provides fast thermal response. Each micromembrane contains a poly-Si doped buried heater embedded in Si_3N_4 with an isolating layer of SiO_2 on the top; Pt interdigitated electrodes are on top of the layers. The details of a very similar platform are described elsewhere [13]. The micromembranes are mounted onto a TO-8 holder, and wire bonded to them.

The synthesis of NWs on top of micromembranes is carried out according to the growth process reported in [14]. A non-continuous Au layer is deposited by 5-10 seconds sputtering and used as a catalyst of the VLS mechanism growth based on the decomposition of the $Sn(O^tBu)_4$ precursor. In order to carry out the growth, the chip with 4 micromembranes is introduced in a quartz-chamber, where the heaters are externally biased while the gaseous precursor is flowing through the chamber. Synthesis is carried out locally only on the heated membranes where the thermal decomposition of the precursor occurs. Low power consumption is required for the growth: 48 mW are needed to achieve this temperature. Growth of NWs takes 30 min including the heating up and cooling down ramps. SnO_2 NWs are grown in low vacuum conditions at a pressure of 0.1 mbar and at temperature around 700 °C.

The response of SnO_2 NWs was characterized in a home-made stainless steel chamber of 8.6 ml volume connected to a Gometrics MGP2 gas mixer with 4 Bronkhorst Mass-Flow Controllers. Constant flow of 200 ml/min was kept both for dry and humid air measurements. Water vapor was added by deviating a part of the synthetic air flow through a bubbler. Relative humidity

provided by the bubbler was calibrated as a function of the air flow before NWs-based sensor characterization using a commercial humidity sensor at 20 °C. The relative humidity conditions indicated throughout the paper are referenced to the RH at room temperature. Keithley 2602A dual Source Measure Unit allowed to control simultaneously the resistance of the sensor and the voltage for heating the micromembrane. Electrical measurements and flowing gases were controlled by a home-developed Labview software.

SnO_2 NWs based gas sensors were characterized towards ammonia by allowing 5 hours to stabilize the baseline, and then first exposing for 1 h to ammonia. The sensors were then exposed to air for 2 h to recover the baseline. This sequence was repeated for the different ammonia concentrations for both dry and humid characterization.

3. Results and discussion

3.1 Temperature behavior in absence of ammonia and humidity

A low magnification SEM image of a micromembrane, where SnO_2 NWs have grown site-selectively, is presented in Fig. 1 (a). The brighter area in this figure denotes the growth of the nanostructures, which also follows the temperature profile provided by the heater. A higher magnification SEM picture of NWs close to the Pt electrode is shown in Fig. 1 (b), where no NWs are found on top of it; a Pt/Au alloy formed during annealing has not acted as a catalyst for nanowires growth.

The crystalline structure of tin dioxide NWs has been analyzed by High Resolution Transmission Electron Microscopy (HRTEM), represented in Fig. 2 (a). As reported in a previous work [14], the locally grown SnO_2 nanowires are monocrystalline, with tetragonal (rutile) phase, with predominant [101] growth direction. A cross-section SEM image of a device with slightly shorter nanowires is shown in Fig. 2 (b), where a high density of NWs is found with a length between 2 and 5 µm, where the contact between the network of NWs can be observed. Besides, a very thin layer is observed between the nanowires and the SiO_2 layer. The two-dimensional growth occurs simultaneously during the synthesis of the nanowires with a much lower growth rate and leads to a nanocrystalline layer of SnO_2 because it is a non-catalyzed process. The thickness of this layer is between 30 and 80 nm and the layer roughness observed is due to the base of nanowires that remained after the sample preparation.

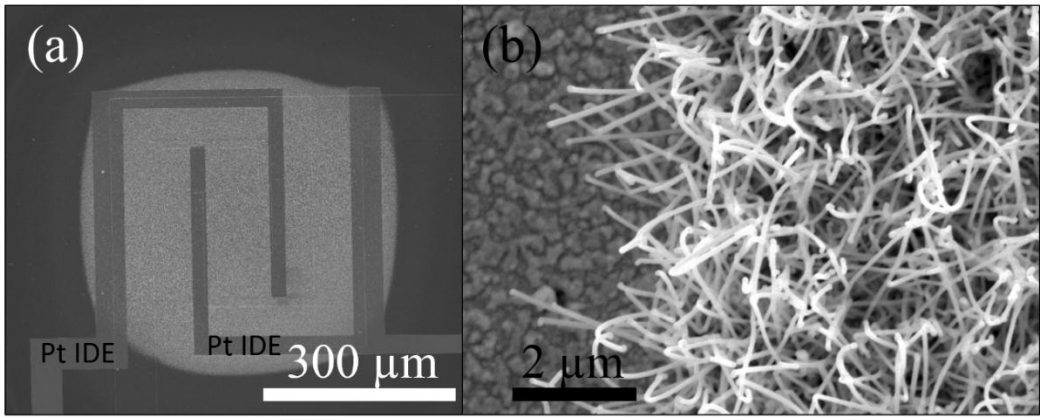

Fig. 1 (a) SEM general view of the micromembrane with Pt interdigitated electrodes (IDE) on the top. Brighter area corresponds to the grown SnO_2 NWs; (b) SEM image of SnO_2 NWs contacting the Pt electrode (on the left side);

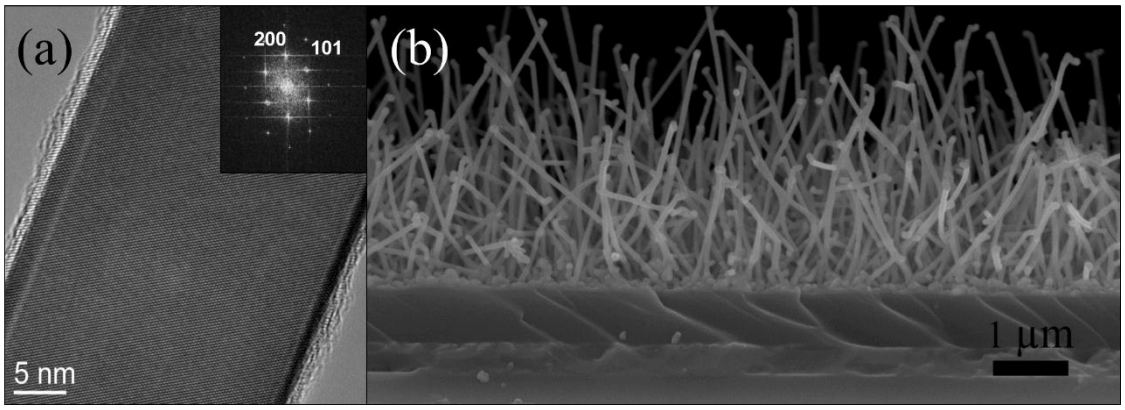

Fig. 2. (a) HR-TEM image of a monocrystalline SnO_2 NW that crystallizes in rutile phase. Inlet FFT illustrates the [101] predominant growth direction; (b) Cross-section of SnO_2 NWs-based sensor. A very thin layer is observed below the NWs of a thickness between 30-80 nm.

The behavior of the electrical resistance of SnO_2 NWs at different temperatures in synthetic air atmosphere has been investigated in order to study the oxygen species that are chemisorbed at the surface of the metal oxide nanostructure (Fig. 3 (a)). The resistance of SnO_2 NWs at room temperature is 2850 Ω, and decreases for increasing temperatures up to 200 °C. Above this temperature and up to 450 °C, the maximum studied temperature, the resistance increases. At temperatures above 500°C, the resistance changes the tendency and decreases for increasing temperatures, which is related to the lower coverage of O^- oxygen species. The same temperature behavior has been obtained in other sensors based on SnO_2 [15]. The SnO_2 nanowires present a low resistance, which is probably due to a highly defective surface. I-V curves of the sensor show an ohmic behavior even at room temperature, which remarks the absence of a Pt/SnO_2 Schottky barrier that would be expected for a pure Pt/SnO_2 interface. The interface between the Pt electrodes and the SnO_2 NWs is partially responsible for a lower resistance than if a Schottky barrier would be present.

At low temperatures atmospheric oxygen is physisorbed [15]. This mechanism takes place without electron transfer and therefore, cannot change the resistivity of the semiconductor. During physisorption, the change in resistance observed is purely due to the excitation of charge carriers. Molecular oxygen (O_2^-) is chemisorbed at the surface at temperatures around 150-200 °C with some degree of charge transfer from the oxide towards the adsorbate. Above 200 °C the oxygen trapped by means of chemisorption can dissociate in two atomic oxygen species (O^-) according to:

$$O_{2(g)}^- + e^- \rightarrow 2O_{(g)}^- \quad (1)$$

Thus, O^- leads to capture more electrons from the semiconductor and thus, increase its resistance [15,16]. The observed resistance behavior has also been reported for other SnO_2 structures at similar temperatures [16]. Therefore, the resistance is related to the particular oxygen species adsorbed at the metal oxide surface. The high temperature range starting at 600 °C renders oxygen atoms that share two electrons (O^{2-}) with the metal oxide [15]. However, these high temperatures are beyond the scope of the present work.

Transient response of the SnO_2 NW device resistance with increasing temperature from 400 to 450 °C is represented in Fig. 3 (b). The low thermal mass of the micromembranes provides a fast thermal response of the order of tens of microseconds to achieve 200 °C [13] which leads to the initial fast decay in resistance when the temperature is changed, but is afterwards followed by a slower increase. The gradual increase in resistance is related to the chemisorption of atomic oxygen species, since temperature changes induce a new dynamic equilibrium between the wire and the adsorbates.

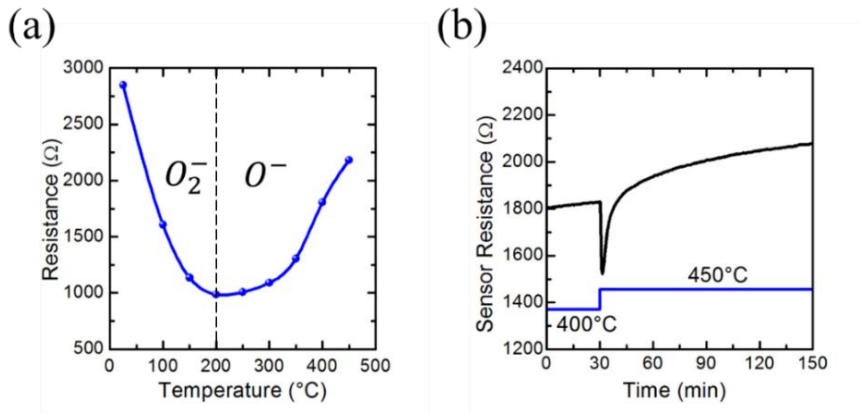

Fig. 3 (a) Resistance of SnO_2 locally grown NWs as a function of temperature. The minimum in resistance reflects the change in the adsorbed oxygen specie; (b) Transient response of the sensor resistance in a change of temperature illustrating the increase in resistance for increasing temperatures above 200 °C. Blue line represents the evolution of temperature.

3.2 Response to ammonia in dry synthetic air

The change in resistance of the locally grown nanowires against ammonia in synthetic air has been measured. The concentration of ammonia has been varied between 10 and 40 ppm, which is in the range of time-weighted average exposure limit recommended by NIOSH (25 ppm) for up-to 10 h workday [17]. The evolution of the sensor resistance at different temperatures is represented in Fig. 4 (a), where the decrease in resistance in the presence of ammonia, expected for an n-type semiconductor gas sensor like tin dioxide, is observed.

The response of the sensor is defined as:

$$Response(\%) = \frac{R_{air} - R_{NH3}}{R_{air}} \quad (2)$$

The response as a function of temperature is represented in Fig. 4 (b). Localized grown SnO_2 NWs show a response of up to 36% for 40 ppm of NH_3 at 400 °C, temperature at which the response presents a maximum. The response time is defined as the time to evolve from 10% to 90% of the steady state value. A response time as low as 2 min is obtained, again, at 400 °C. An Arrhenius plot of the response time as a function of temperature is represented in Fig. 4 (c), where an exponential behavior is deduced.

Three competitive reactions are described in the literature for ammonia oxidation on metal oxide surfaces [18–20]:

$$\alpha 2NH_{3\,(g)} + 3O^-_{\alpha\,(s)} \rightarrow \alpha N_{2(g)} + \alpha 3H_2O_{(g)} + 3e^- \qquad T < 400\,°C \quad (3)$$

$$\alpha 2NH_{3\,(g)} + 4O^-_{\alpha\,(s)} \rightarrow \alpha N_2O_{(g)} + \alpha 3H_2O_{(g)} + 4e^- \qquad T < 400\,°C \quad (4)$$

$$\alpha 2NH_{3\,(g)} + 5O^-_{\alpha\,(s)} \rightarrow \alpha 2NO_{(g)} + \alpha 3H_2O_{(g)} + 5e^- \qquad T > 400\,°C \quad (5)$$

where (g) stands for gas, (s) for surface, e^- is a conduction electron, α is a coefficient that is equal to 1 for atomic oxygen O^- or 2 for molecular oxygen O_2^- ionosorbed species and consequently, depends on the working temperature. The three reaction mechanisms are supported by chemisorbed oxygen at the surface of the metal oxide. Our work is focused at temperatures above 200 °C in order to achieve acceptable response time for the gas sensing and, as a consequence, chemisorbed atomic oxygen is the specie that oxidizes ammonia molecules at the surface of the SnO_2 nanowires.

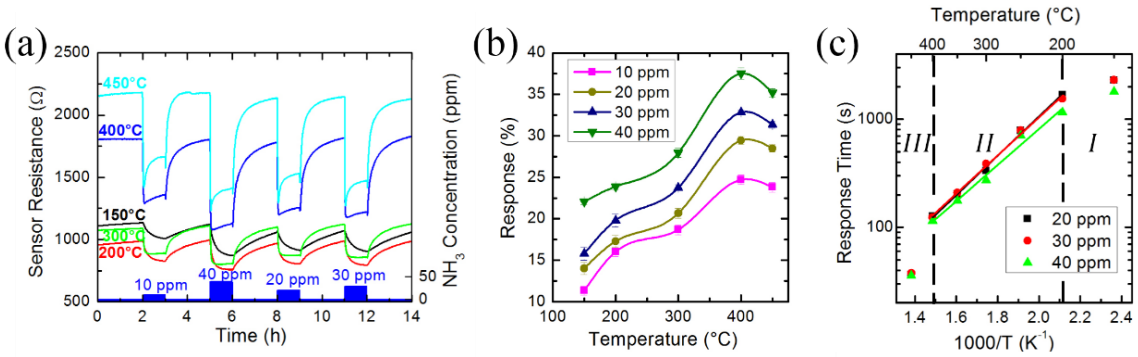

Fig. 4. (a) Evolution of SnO_2 NWs resistance in front of different concentration of ammonia in synthetic air; (b) Response of the test represented in a) in function of temperature; (c) Arrhenius plot of the response time for pulses of 30 ppm of NH_3. Symbols are experimental values and lines are the fitted exponential decay.

It is well known from catalysis that in a large number of metal oxide catalysts, depending on the temperature one specific reaction is preferred over the others [20,21]. In this direction, the sensing equations (3-5) are by no means easy to disentangle. Indeed, these reactions account for oxygen adsorption in the form of the active species and subsequent H stripping from the ammonia molecules till a relevant intermediate containing the NN or NO bond is formed. When this takes place, further H elimination with the concomitant formation of H_2O is carried out. Thus, equations (3-5) share more than 70% of their elementary steps. Consequently, in the low temperature regime, i.e., below 400 °C approximately, the reactions (3) and (4) take place simultaneously.

Reaction (5) dominates at temperatures above 400 °C and surface coverage governs the reaction since higher energy barriers can be surpassed at this temperature, the NO byproduct becomes dominant [20,21]. The nitrogen containing products of the three reactions are therefore oxidized as a function of temperature: the higher the temperature at which the reaction takes place, the more oxidized is the nitrogen containing product. At the same time, the more oxidized is the nitrogen product also the higher the activation energy, following the relationship $E_{(3)}^{act} < E_{(4)}^{act} < E_{(5)}^{act}$ [20].

The activation energy of the sensor response towards ammonia has been obtained from the response time, which is represented as a function of temperature in Fig. 4 (c) in an Arrhenius plot. Three different kinetic regions are defined from the plot according to the experimental measurements: I) temperatures below 200 °C; II) between 200 and 400 °C and III) above 400 °C, each of them with different activation energies.

The main reaction that takes place at lower temperatures (region I) is ammonia oxidation involving molecular oxygen ions, since this species is the main oxygen form at this temperature range, which gives a different activation energy to the one deduced from region II. Activation energy from this region cannot be derived due to the small number of points measured, but a lower slope than region II in the τ(1000/kT) is traced. The activation energy obtained from Arrhenius plot in region II is $E_{II}^{act} = 0.35 \pm 0.04eV$, where ammonia oxidation is supported by atomic oxygen. This process was also found to provide higher activation energy than molecular oxygen in [22]. Therefore, differences in sensing kinetics are explained by the different oxygen species promoting the NH_3 oxidation.

On the other hand, this region comprehends the temperature range where reactions (3) and (4) can take place on the tin dioxide surface. The exponential behavior of the response time in the Arrhenius plot suggests that the same mechanism takes place over the whole temperature range.

As pointed out before, both mentioned reactions can occur simultaneously at these temperatures; both share many elementary steps and the rate determining step O_2 activation is the same and, thus, a unique dependence is found. Furthermore, the ratio between oxygen and ammonia partial pressures (p_{O2}/p_{NH3}) also influences the selectivity towards one of the three reactions. As shown in [20], for $p_{O2}/p_{NH3}>10$, the selectivity is lost and N_2 and N_2O are produced in equivalent percentage at temperatures below 400 °C. On the other hand, for low p_{O2}/p_{NH3} ratios (<0.1), N_2 production is enhanced [18,20], and N_2O production is almost negligible. Consequently, as our experiments are carried out in high p_{O2}/p_{NH3}, sensing mechanism in region II can be considered as the addition of reactions (3) and (4) taking place in parallel.

The activation energy detailed in this work is lower than in [20] and in a previous work [23], which obtained an activation enthalpy of 0.74 eV (range between 210-260 °C, reaction mixture of 10% of ammonia and 90% of O_2) and 0.5 eV (150-300 °C), respectively. The study of SnO_2 as a catalyst for NH_3 oxidation concluded that the formation of reaction (3) started at temperatures below 200 °C, and reaction (4) takes place for temperatures higher than 200 °C [20]. Furthermore, in previous density functional theory (DFT) studies we concluded that the rate-determining step of NH_3 sensing mechanism in a single SnO_2 monocrystalline nanowire is oxygen adsorption, with an associated activation energy of 0.5 eV, similar to the experimental value obtained in that work [23]. Notice, though that the errors intrinsic to DFT in particular when dealing with the description of O_2 make the DFT value a qualitative estimate. Still, if oxygen adsorption is energetically favored, i.e. oxygen binding energy to the surface increases, then the activation energy of the whole process could be lowered.

A change in tendency of the response time as a function of temperature is observed again at 450 °C in Fig. 4 (c), the labelled region III. The variation in transient behavior at 450 °C suggests that a different reaction takes place, which could correspond to reaction (5), since this latter starts to dominate at about 400 °C. The temperature intervals for NO reaction are in agreement with other works, and are also supported by the transient decay of the sensor resistance at 400 and 450 °C. The initial interaction of ammonia with the metal oxide surface leads to a fast decay of the NWs resistance at these temperatures, followed by a slow increase during the exposure to NH_3. The same behavior has also been observed in metal oxide sensors like WO_3 [19] and In_2O_3/MgO bilayer structure [24] in the characterization of their responses towards ammonia.

Nitric oxide (NO) is easily and readily oxidized to NO_2 at 400 °C [24,25]. SnO_2 NWs are known to respond to less than 100 ppb of NO_2 [26], a value easy to reach during the ammonia and nitric oxide oxidation. Other products generated in the reactions cannot explain the observed increasing resistance. On the one hand, H_2O acts as a reducing agent to tin dioxide, i.e., diminishes the resistance of tin oxide NWs and, consequently, as a product of reaction (3), (4) and (5), could not provide the increase in resistance. N_2 is inert at the analyzed temperature range and does not affect the conductivity. Furthermore, SnO_2 without additives on its surface requires tens of ppm of N_2O [27] to achieve an observable response. As a result, the only reaction that will give rise to the observed behavior is the oxidation of NO to NO_2, which is the only species able to promote the increasing resistance. Thus, NO_2 attaches to an oxygen vacancy at the SnO_2 surface [28], trapping an electron and therefore the resistance of SnO_2 is increased as a consequence of the reactions:

$$2NO_{(g)} + O_2 \rightarrow 2NO_{2(g)} \quad (6)$$

$$NO_{2\,(g)} + e^- \rightarrow NO^-_{2(s)} \quad (7)$$

This fact is confirmed by the reduction of the response for temperatures above 400 °C. Actually, the initial resistance decay towards ammonia at 450 °C is larger than the decay when the sensor

is heated at 400 °C. However, the further resistance increase due to NO_2 adsorption reduces the final response (see Fig. 5 (d)). Therefore, at this temperature the response of the sensor is explained by reactions (5), (6) and (7) that take place simultaneously, being (6) and (7) secondary reactions.

The observed low resistance of the NWs network at room temperature is an indicator of the presence of surface defects, i.e., that oxygen vacancies are widely present at the surface of the NWs. Consequently, the gas response is probably lowered partially since chemisorbed oxygen is necessary for the ammonia sensing mechanism, as reactions (3) (4) and (5) describe.

3.3 SnO_2 NWs sensing mechanisms in humid conditions

3.3.1. SnO_2 NWs interaction towards H_2O

SnO_2 NWs exhibit a reversible response towards different concentration of water vapor at different examined temperatures. Water vapor is expressed as relative humidity in %, i.e., the ratio of partial water vapor pressure and saturation pressure obtained at room temperature (20 °C). The transient in electrical signal of the sensor towards the presence of water vapor is shown in Fig. 5 (a) at an operation temperature of 400 °C. A clear decrease in resistance due to the presence of water vapor is observed, which is reversible as can be seen in the same figure since the baseline value is fully recovered when water vapor is removed from the chamber.

The behavior of the NWs resistance as a function of the relative humidity denotes that water vapor acts as a reducing gas for SnO_2 nanostructures. SnO_2 NWs have been reported as high sensitivity humidity sensor [29]. There are several mechanisms reported in literature for the interaction of H_2O with the tin dioxide surface. Dissociation of water involves the reaction of hydroxyl groups with oxygen atoms from the lattice, providing terminal OH group, and thus, releasing two electrons per molecule to the conduction band according to the following equation [30–32]:

$$H_2O + 2Sn_{lat} + O_{lat} \leftrightarrow 2(OH - Sn_{lat}) + V_{\ddot{O}} + 2e^- \quad (8)$$

where Sn_{lat} and O_{lat} stands for a tin and oxygen atom in lattice position, respectively, and $V_{\ddot{O}}$ is a doubly ionized oxygen vacancy. Another mechanism related to chemisorbed oxygen at the SnO_2 surface is the competitive reaction of water with pre-adsorbed oxygen ions, which is similar to equation (8), but involved oxygen is an atomic chemisorbed specie that releases an electron to the metal oxide [30]:

$$H_2O + 2Sn_{lat} + O^-_{(s)} \leftrightarrow 2(OH - Sn_{lat}) + e^- \quad (9)$$

Equation (9) is supported by diffuse reflectance infrared Fourier transform (DRIFT) spectroscopy measurements that conclude that only OH terminal groups are formed at the surface of SnO_2 [30]. The authors observed that the concentration of these surface hydroxyl groups increased with oxygen partial pressure, reaching a saturation, and showed that this effect was reversible. Therefore, the concentration of hydroxyl groups which provides the increase in conductivity to the metal oxide is strongly dependent on chemisorbed oxygen. Consequently, when another reducing gas is present, together with H_2O, both will compete for reacting with chemisorbed oxygen atoms.

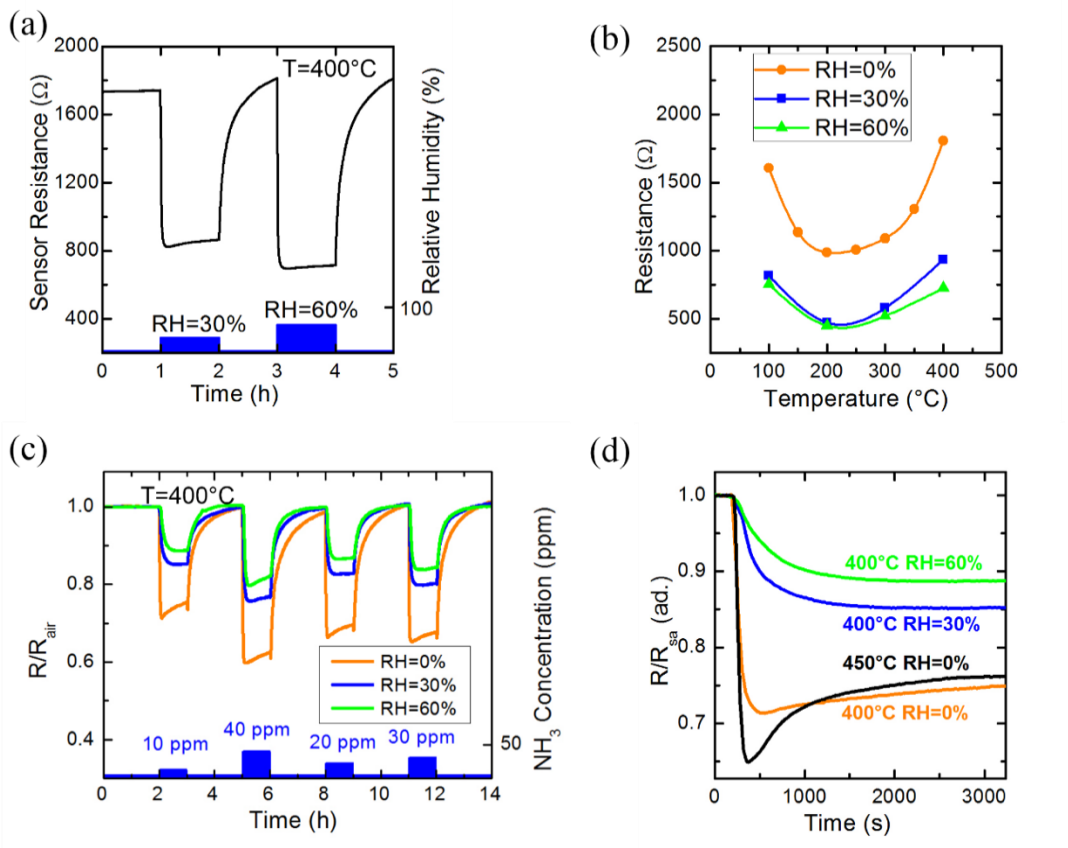

Fig. 5 (a) Electrical response of SnO_2 NWs to different concentrations of water vapor in synthetic air at 400 °C; (b) Resistance of SnO_2 NWs for different humidity levels at different temperature. U-shaped R-T is also obtained in humid conditions due to dissociation of molecular to atomic oxygen at a temperature of 200 °C; (c) Electrical response of SnO_2 NWs in dry, 30% and 60% of relative humidity (RH at room temperature) towards different ammonia pulses in synthetic air. Three tests have been performed by keeping 400 °C constant temperature; (d) Sensor response towards 10 ppm of NH_3 at different conditions. The overshoot in resistance is visible for 450 °C and RH=0% curve.

The resistance as a function of temperature in both dry and humid conditions (30% and 60% of relative humidity) is represented in Fig. 5 (b). As can be seen, the sensor resistance decreases at higher concentrations of water vapor. On the other hand, resistance of SnO_2 NWs grows with increasing temperature above 200 °C, showing a U-shaped resistance-temperature curve. The increasing resistance ensures that atomic oxygen is available to react with other species; there is an incomplete coverage of chemisorbed oxygen with hydroxyl groups since otherwise, a decreasing resistance for increasing temperature would be experimentally observed.

3.3.2 Ammonia sensing in humid conditions

Sensing capabilities of tin dioxide nanowires towards ammonia added to water vapor have been investigated at a temperatures of 200, 300 and 400 °C, where mainly atomic oxygen is chemisorbed at the semiconductor's surface. Two different relative humidity levels were employed for each temperature: 30 and 60% for the same sequence of ammonia pulses performed in dry air experiments.

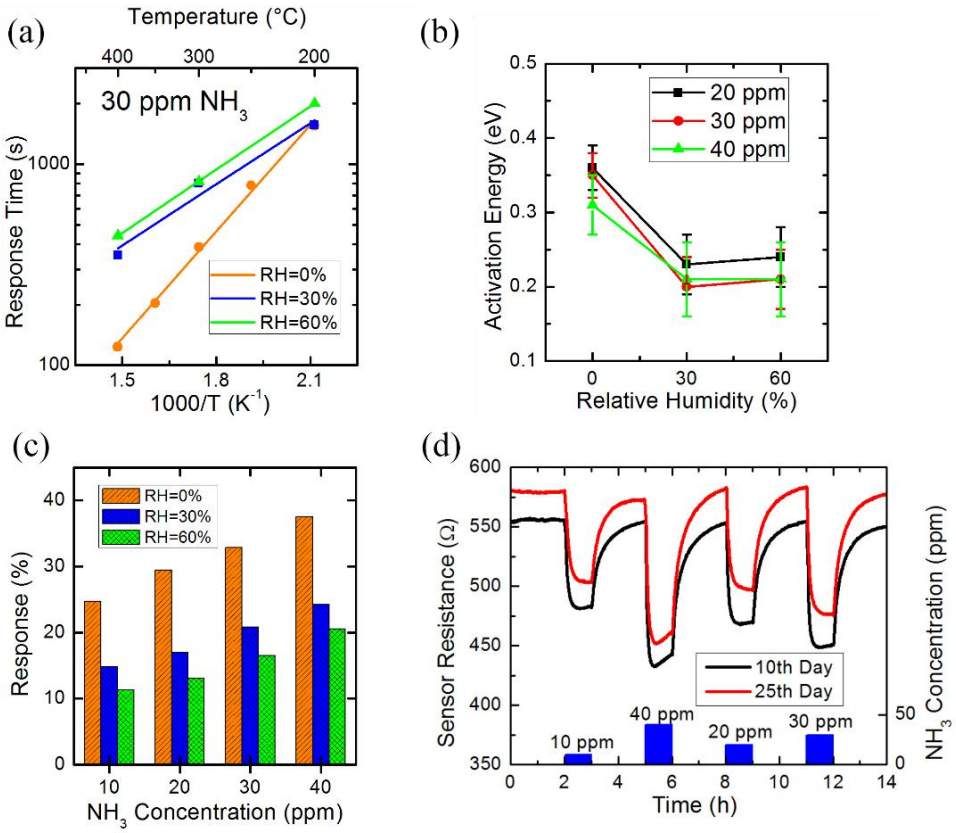

Fig. 6 (a) Response time of sensor of NH_3 pulses of 30 ppm in dry and humid condition, represented in an Arrhenius plot. Symbols are experimental values and lines are the fitted exponential decay; (b) Activation energy obtained from response time for ammonia response in function of relative humidity, for all the concentrations studied; (c) Response in humid condition of SnO_2 NWs against ammonia at 400 °C. The sensor distinguishes the concentration of ammonia in a precision of 30 ppm in realistic operational conditions, where humidity is present; (d) Comparison between the response of the sensor at 300 °C and 30% of RH from 10^{th} and 25^{th} day of measurements. A change of 5% in resistance baseline is obtained.

The normalized sensor resistance to the baseline value in synthetic air at 400 °C is represented in Fig. 5 (c) for dry and humid conditions towards different concentrations of ammonia. Clearly, the response is reduced in the presence of increasing amounts of water as compared to dry conditions. The sensor resistance does not show the overshoot in resistance observed in the response towards ammonia in dry conditions at 450 °C (see Fig. 5 (d) for comparison), suggesting that reactions (3) and (4) are the main ones that take place in the studied range, and the influence of (5) is here negligible.

The reduced response of tin dioxide nanowires against ammonia in the presence of water vapor can be explained by several concurring mechanisms. On the one hand, competitive adsorption between water vapor and ammonia with chemisorbed oxygen takes place. Atomic oxygen and water vapor compete for the same adsorption sites, diminishing the probability of reactions (3), (4) and (5) in the steady sensing state. Furthermore, 60% of relative humidity at 20 °C corresponds to approximately 14300 ppm of water, a concentration 3 orders of magnitude higher than ammonia in these experiments. Thus, the partial pressure of water is considerably higher than that of ammonia, which leads to much higher coverage of these adsorbed species on the metal oxide surface.

The Arrhenius plot of the response time of the sensor in dry and humid conditions for 30 ppm of ammonia (Fig. 6 (a)) shows that the response is slower in humid than in dry conditions, and that the higher the temperature, the higher the difference. Larger response times are a direct consequence of the competitive adsorption between atomic oxygen and water vapor that reduces

the probability of oxidizing ammonia and, thus, slows down the reaction. The effect is more pronounced at higher temperatures because under dry conditions the reaction is promoted without any competitive adsorption phenomenon.

At the same time, the activation energies shown in Fig. 6 (b), deduced from Fig. 6 (a) for different ammonia concentrations and in the different studied relative humidity values, clearly decrease in the presence of water vapor and are essentially independent on the ammonia concentration, within the experimental uncertainty. As mentioned before, water vapor can dissociate in two hydroxyl species and chemisorb at the surface of tin oxide assisted by a Sn_{lat} and a chemisorbed $O^-_{(s)}$ as described in (8). A tentative explanation for the behavior could be derived from the interaction of hydroxyl groups with O_2, as proposed by Epling *et al.* [33,34] in monocrystalline rutile TiO_2 according to:

$$OH_{(s)} + O_{2(g)} \rightarrow O^-_{(s)} + (O_a - OH)_{(s)} \quad (9)$$

where O_a stands for an oxygen adatom. This mechanism creates a new path for oxygen dissociation, which can occur even at lower temperatures than oxygen dissociation described in (1), diminishing the activation barrier of oxygen dissociation. According to our previous study of ammonia interaction mechanism, oxygen dissociation is precisely the energy limiting step [23]. Thus, a mechanism similar to (9) could explain the lowering in the activation energy of ammonia sensing in presence of water. There is an extra term of adsorbed oxygen (O_a) which grows with increasing number of OH groups at the surface that can act as H scavenging centers, thus improving the probability of adsorbed ammonia to react with active bases in the intermediate ammonia decomposition steps.

As for endurance, the sensors were operated for 1 month in dry and humid conditions, after which a drift in resistance of 7% from the initial values was observed, but where the resistance change due to the presence of the gases was almost invariant in its value, only about 1%. Fig. 6 (d) shows the resistance change at 300 °C and 30% of RH obtained at the 10^{th} and 25^{th} day of operation, and illustrates the repeatability of measurements made with the nanowire-based device. The sensor has shown a good durability, and offers relatively fast response times of 6 minutes in presence of water vapor, and 2 minutes for dry conditions towards 30 ppm of NH_3.

4. Conclusions

The sensing mechanisms of locally grown SnO_2 NWs towards ammonia gas diluted in air, in both dry and humid conditions, have been studied. Different temperature regimes have been identified in the sensor kinetic response. In dry conditions, the promotion of NO as byproduct at high operating temperatures reduces the response of the sensor and provides a maximum ammonia response at 400 °C. When operated in humid conditions, the response of tin dioxide nanostructures is reduced and slowed down by the presence of water vapor. Simultaneously, the activation energy is lowered by moisture, which could be explained through the reaction between O_2 and the OH adsorbed groups, consequence of water decomposition. Finally, the integrated growth of SnO_2 on micromembranes has been demonstrated as a fast, reproducible and low power consuming approach, which gives rise to ammonia sensors with good repeatability, fast response and long term stability.

Acknowledgements

The research leading to these results has received funding from the Spanish Ministerio de Economía y Competitividad, through project TEC2013-48147-C6 (TEMIN-AIR) and from the European Research Council under the European Union's Seventh Framework Programme (FP/2007-2013) / ERC Grant Agreement n. 336917. J.D. Prades acknowledges the support of the Serra Húnter Program. Transmission electron microscopy investigations were carried out

using facilities at the University Service Centre for Transmission Electron Microscopy, Vienna University of Technology, Austria.

References

[1] T.M. Banhazi, J. Seedorf, D.L. Rutley, W.S. Pitchford, Identification of risk factors for sub-optimal housing conditions in Australian piggeries: Part 1. Study justification and design, J. Agric. Saf. Health. 14 (2008) 5–20.

[2] J.N. Galloway, F.J. Dentener, D.G. Capone, E.W. Boyer, R.W. Howarth, S.P. Seitzinger, et al., Nitrogen cycles: Past, present, and future, 2004. doi:10.1007/s10533-004-0370-0.

[3] F.-X. Philippe, J.-F. Cabaraux, B. Nicks, Ammonia emissions from pig houses: Influencing factors and mitigation techniques, Agric. Ecosyst. Environ. 141 (2011) 245–260. doi:10.1016/j.agee.2011.03.012.

[4] S. Brandenberger, O. Kröcher, A. Tissler, R. Althoff, The State of the Art in Selective Catalytic Reduction of NOx by Ammonia Using Metal-Exchanged Zeolite Catalysts, Catal. Rev. 50 (2008) 492–531. doi:10.1080/01614940802480122.

[5] M. Mehring, M. Elsener, O. Kröcher, Diesel soot catalyzes the selective catalytic reduction of NOx with NH3, Top. Catal. 56 (2013) 440–445. doi:10.1007/s11244-013-9993-5.

[6] N. Taguchi, Patent, 45-38200, 1962.

[7] N. Yamazoe, New approaches for improving semiconductor gas sensors, Sensors Actuators B Chem. 5 (1991) 7–19. doi:10.1016/0925-4005(91)80213-4.

[8] S. Barth, F. Hernandez-Ramirez, J.D. Holmes, A. Romano-Rodriguez, Synthesis and applications of one-dimensional semiconductors, Prog. Mater. Sci. 55 (2010) 563–627. doi:10.1016/j.pmatsci.2010.02.001.

[9] F. Hernandez-Ramirez, J.D. Prades, a Tarancon, S. Barth, O. Casals, R. Jiménez–Diaz, et al., Portable microsensors based on individual SnO_2 nanowires, Nanotechnology. 18 (2007) 495501. doi:10.1088/0957-4484/18/49/495501.

[10] D.T.T. Le, N. Van Duy, H.M. Tan, D.D. Trung, N.N. Trung, P.T.H. Van, et al., Density-controllable growth of SnO2 nanowire junction-bridging across electrode for low-temperature NO2 gas detection, J. Mater. Sci. 48 (2013) 7253–7259. doi:10.1007/s10853-013-7545-9.

[11] J. Guilera, C. Fàbrega, O. Casals, F. Hernández-Ramírez, S. Wang, S. Mathur, et al., Facile integration of ordered nanowires in functional devices, Sensors Actuators B Chem. 221 (2015) 104–112. doi:10.1016/j.snb.2015.06.069.

[12] S. Mathur, S. Barth, H. Shen, J.-C. Pyun, U. Werner, Size-Dependent Photoconductance in SnO2 Nanowires, Small. 1 (2005) 713–717. doi:10.1002/smll.200400168.

[13] J. Puigcorbé, D. Vogel, B. Michel, A. Vilà, I. Gràcia, C. Cané, et al., Thermal and mechanical analysis of micromachined gas sensors, J. Micromechanics Microengineering. 13 (2003) 548–556. doi:10.1088/0960-1317/13/5/304.

[14] S. Barth, R. Jimenez-Diaz, J. Samà, J. Daniel Prades, I. Gracia, J. Santander, et al., Localized growth and in situ integration of nanowires for device applications, Chem. Commun. 48 (2012) 4734–4736. doi:10.1039/c2cc30920c.

[15] S. Ahlers, T. Becker, W. Hellmich, C. Braunmühl, G. Müller, Temperature- and Field-Effect-Modulation Techniques for Thin-Film Metal Oxide Gas Sensors, in: T. Doll (Ed.), Adv. Gas Sens. SE - 6, Springer US, 2003: pp. 123–159. doi:10.1007/978-1-4419-8612-2_6.

[16] S. Chang, Oxygen chemisorption on tin oxide: Correlation between electrical

conductivity and EPR measurements, J. Vac. Sci. Technol. 17 (1980) 366. doi:10.1116/1.570389.

[17] National Institute for Occupational Safety and Health (NIOSH), NIOSH Pocket Guide to Chemical Hazards - Human Services, Saf. Heal. (2007).

[18] M. de Boer, H.M. Huisman, R.J.M. Mos, R.G. Leliveld, a. J. van Dillen, J.W. Geus, Selective oxidation of ammonia to nitrogen over SiO2-supported MoO3 catalysts, Catal. Today. 17 (1993) 189–200. doi:10.1016/0920-5861(93)80023-T.

[19] I. Jiménez, M.A. Centeno, R. Scotti, F. Morazzoni, J. Arbiol, A. Cornet, et al., NH3 interaction with chromium-doped WO3 nanocrystalline powders for gas sensing applications, J. Mater. Chem. 14 (2004) 2412. doi:10.1039/b400872c.

[20] N.I. Il'chenko, Catalytic Oxidation of Ammonia, Russ. Chem. Rev. 45 (1976) 1119–1134. doi:10.1070/RC1976v045n12ABEH002765.

[21] V.A. Sadykov, L.A. Isupova, I.A. Zolotarskii, L.N. Bobrova, A.S. Noskov, V.N. Parmon, et al., Oxide catalysts for ammonia oxidation in nitric acid production: properties and perspectives, Appl. Catal. A Gen. 204 (2000) 59–87. doi:10.1016/S0926-860X(00)00506-8.

[22] C.-M. Hung, Decomposition kinetics of ammonia in gaseous stream by a nanoscale copper-cerium bimetallic catalyst, J. Hazard. Mater. 150 (2008) 53–61. doi:10.1016/j.jhazmat.2007.04.044.

[23] F. Shao, M.W.G. Hoffmann, J.D. Prades, J.R. Morante, N. López, F. Hernández-Ramírez, Interaction mechanisms of ammonia and Tin oxide: A combined analysis using single nanowire devices and DFT calculations, J. Phys. Chem. C. 117 (2013) 3520–3526. doi:10.1021/jp3085342.

[24] Y. Takao, High Ammonia Sensitive Semiconductor Gas Sensors with Double-Layer Structure and Interface Electrodes, J. Electrochem. Soc. 141 (1994) 1028. doi:10.1149/1.2054836.

[25] K. Skalska, J.S. Miller, S. Ledakowicz, Kinetics of nitric oxide oxidation, Chem. Pap. 64 (2010) 269–272. doi:10.2478/s11696-009-0105-8.

[26] J.D. Prades, R. Jimenez-Diaz, F. Hernandez-Ramirez, S. Barth, A. Cirera, A. Romano-Rodriguez, et al., Ultralow power consumption gas sensors based on self-heated individual nanowires, Appl. Phys. Lett. 93 (2008) 123110. doi:10.1063/1.2988265.

[27] E. Kanazawa, G. Sakai, K. Shimanoe, Y. Kanmura, Y. Teraoka, N. Miura, et al., Metal oxide semiconductor N2O sensor for medical use, Sensors Actuators, B Chem. 77 (2001) 72–77. doi:10.1016/S0925-4005(01)00675-X.

[28] P.T. Moseley, Solid state gas sensors, Meas. Sci. Technol. 8 (1997) 223. http://stacks.iop.org/0957-0233/8/i=3/a=003.

[29] F. Hernandez-Ramirez, S. Barth, A. Tarancon, O. Casals, E. Pellicer, J. Rodriguez, et al., Water vapor detection with individual tin oxide nanowires., Nanotechnology. 18 (2007) 424016. doi:10.1088/0957-4484/18/42/424016.

[30] D. Koziej, N. Bârsan, U. Weimar, J. Szuber, K. Shimanoe, N. Yamazoe, Water-oxygen interplay on tin dioxide surface: Implication on gas sensing, Chem. Phys. Lett. 410 (2005) 321–323. doi:10.1016/j.cplett.2005.05.107.

[31] S.H. Hahn, N. Bârsan, U. Weimar, S.G. Ejakov, J.H. Visser, R.E. Soltis, CO sensing with SnO2 thick film sensors: Role of oxygen and water vapour, Thin Solid Films. 436 (2003) 17–24. doi:10.1016/S0040-6090(03)00520-0.

[32] G. Heiland, D. Khol, Physical and Chemical Aspects of Oxidic Semiconductor Gas Sensors, Kodansha Ltd, 1988. doi:10.1016/B978-0-444-98901-7.50007-5.

[33] W.S. Epling, C.H.F. Peden, M.A. Henderson, U. Diebold, Evidence for oxygen adatoms

on TiO2(110) resulting from O2 dissociation at vacancy sites, Surf. Sci. 412-413 (1998) 333–343. doi:10.1016/S0039-6028(98)00446-4.

[34] M.A. Henderson, W.S. Epling, C.H.F. Peden, C.L. Perkins, Insights into Photoexcited Electron Scavenging Processes on TiO 2 Obtained from Studies of the Reaction of O 2 with OH Groups Adsorbed at Electronic Defects on TiO 2 (110), J. Phys. Chem. B. 107 (2003) 534–545. doi:10.1021/jp0262113.